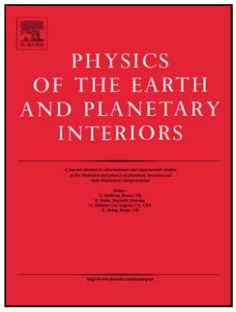

Title: Tidal instability in stellar and planetary binary systems

Authors: M. Le Bars, L. Lacaze, S. Le Dizès, P. Le Gal, M. Rieutord

PII: S0031-9201(09)00148-4
DOI: doi:10.1016/j.pepi.2009.07.005
Reference: PEPI 5180

To appear in: *Physics of the Earth and Planetary Interiors*

Received date: 18-12-2008
Revised date: 20-5-2009
Accepted date: 1-7-2009

Please cite this article as: Le Bars, M., Lacaze, L., Le Dizès, S., Le Gal, P., Rieutord, M., Tidal instability in stellar and planetary binary systems, *Physics of the Earth and Planetary Interiors* (2008), doi:10.1016/j.pepi.2009.07.005

Tidal instability in stellar and planetary binary systems

M. Le Bars*[,a], L. Lacaze[b], S. Le Dizès[a], P. Le Gal[a], M. Rieutord[c]

[a] *Institut de Recherche sur les Phénomènes Hors Equilibre, UMR 6594, CNRS et Aix-Marseille Université, 49 rue F. Joliot-Curie, BP146, 13384 Marseille Cédex 13, France.*

[b] *Institut de Mécanique des Fluides de Toulouse, CNRS et Université de Toulouse, 1 Allée du Professeur Camille Soula, 31400 Toulouse, France.*

[c] *Laboratoire d'Astrophysique de Toulouse-Tarbes, CNRS et Université de Toulouse, 14 avenue E. Belin, 31400 Toulouse, France*

Abstract

In this paper, we combine theoretical and experimental approaches to study the tidal instability in planetary liquid cores and stars. We demonstrate that numerous complex modes can be excited depending on the relative values of the orbital angular velocity Ω_{orbit} and of the spinning angular velocity Ω_{spin}, except in a stable range characterized by $\Omega_{spin}/\Omega_{orbit} \in [-1; 1/3]$. Even if the tidal deformation is small, its subsequent instability - coming from a resonance process - may induce motions with large amplitude, which play a fundamental role at the planetary scale. This general conclusion is illustrated in the case of Jupiter's moon Io by a coupled model of synchronization, demonstrating the importance of energy dissipation by elliptical instability.

Key words: tides, tidal/elliptical instability, synchronization, binary systems

*corresponding author

Email address: lebars@irphe.univ-mrs.fr (M. Le Bars)

1. Introduction

The fundamental role of tides in geo- and astrophysics has been the subject of multiple studies for more than four centuries. Beyond the well-known quasi-periodic flow of ocean water on our shores, tides are also responsible for phenomena as varied as the intense volcanism on Io or the synchronization of the Moon on Earth. In stars and liquid planetary cores, tides may also excite an hydrodynamic "elliptical" instability, whose consequences are not yet fully understood. The purpose of the present work is twofold: we shall first systematically characterize the excited modes of the elliptical (or tidal) instability in a rotating spheroid depending on its orbital and spinning velocities, and then demonstrate the importance of this instability in stellar and planetary binary systems using a simplified but illustrative model of tidal synchronization.

The elliptical instability, whose existence is related to a parametric resonance of inertial waves, is well-known in aeronautics, and more generally in the field of vortex dynamics: it actually affects any rotating fluid, as soon as its streamlines are elliptically deformed. Since its discovery in the mid-1970s, the elliptical instability has received considerable attention, theoretically, experimentally and numerically (see for instance the review by Kerswell, 2002). Its presence in planetary and stellar systems, elliptically deformed by gravitational tides, has been suggested for several years. It could for instance be responsible for the surprising existence of a magnetic field in Io (Kerswell and Malkus, 1998; Lacaze et al., 2006; Herreman et al., 2009) and for fluctuations in the Earth's magnetic field on a typical timescale of 10,000 years (Aldridge et al., 1997). It may also have a significant influence on the evolution of

binary stars (e.g. Rieutord, 2003).

In all these studies, it is assumed that the tidal deformation is fixed and that the excited resonance is the so-called spin-over mode, which corresponds to a solid body rotation around an axis inclined compare to the spin axis of the system. This is indeed the only perfect resonance in spherical geometry in the absence of rotation of the elliptical deformation (Lacaze et al., 2004). But in all natural configurations such as binary stars, moon-planet systems or planet-star systems, orbital motions are also present, which means that the gravitational interaction responsible for the tidal deformation is rotating with an angular velocity and/or a direction different from the spin of the considered body. This significantly changes the conditions for resonance and the mode selection process, as recently demonstrated in the cylindrical geometry (Le Bars et al., 2007).

The paper is organized as follow. In section 2, in complement to the trends presented in Le Bars et al. (2007), we systematically characterize the excited modes of the elliptical instability in a rotating spheroid depending on its orbital and spinning velocities, using both theoretical and experimental approaches. We then describe in section 3 a fully coupled simplified model of synchronization of stellar and planetary binary systems, demonstrating the importance of energy dissipation by elliptical instability. In the last section, the main results of the paper are summarized and general conclusions for geo- and astrophysical systems are briefly discussed.

2. Excited modes of the elliptical instability in an orbiting spinning spheroid

Our study is based on the laboratory experiment shown in figure 1a. The set-up consists in a deformable and transparent hollow sphere of radius $R = 2.175$cm, set in rotation about its axis (Oz) with an angular velocity Ω_F up to ± 300rpm, simultaneously deformed elliptically by two fixed rollers parallel to (Oz). The container is filled with water seeded with anisotropic particles (Kalliroscope). For visualization, a light sheet is formed in a plane coinciding with the rotation axis, allowing the measurement of wavelengths and frequencies of excited modes. The whole set-up is placed on a 0.5m-diameter rotating table allowing rotation with an angular velocity Ω_{orbit} up to 60rpm. Such a system is fully defined by three dimensionless numbers: ε, the eccentricity of the tidal deformation, $\Omega = \Omega_{orbit}/\Omega_F$, the ratio between the orbital and the fluid angular velocities, and $E = \nu/\Omega_F R^2$, an Ekman number, where ν is the kinematic viscosity of the fluid. In geo- and astrophysical terms, this toy model mimics a tidally deformed fluid body spinning at $\Omega_{spin} = \Omega_F + \Omega_{orbit}$ with a tidal deformation rotating at the orbital velocity Ω_{orbit} (see figure 1b). Note that in natural configurations, the gravitational interactions responsible for the boundary deformation of the considered planet or star also act over the whole depth of the system. This feature cannot be taken into account in our toy model. However, it touches another side of the problem, namely the role of compressibility and stratification which we leave for subsequent studies. We focus here on incompressible effects only, considering a fluid of uniform density.

2.1. Linear global analysis

As previously mentioned, the elliptical instability is generated by the parametric resonance of two normal modes of the undistorted circular flow with the underlying strain field (e.g. Waleffe, 1990; Kerswell, 2002). We have thus performed a so-called "global" analysis of the instability, which consists in (i) determining the normal modes of the sphere, (ii) calculating explicitly the conditions for resonance, which immediately provides information on the structure of the selected instability and (iii) determining the growth rate of this instability. In the following, we work in the frame rotating with the rotating table (i.e. in the frame where the elliptical deformation is stationary), and variables are nondimensionalized using the characteristic lengthscale R and the characteristic timescale $1/\Omega_F$ (i.e. the relevant timescale for the elliptical instability, corresponding to the differential rotation of the fluid compared to the elliptical deformation).

As explained in Le Bars et al. (2007), inviscid normal modes in a rotating container submitted to a global rotation Ω are related to inviscid normal modes without global rotation through the relation

$$\{\mathbf{u}, p\}(\omega, \Omega, m, l) = \{\frac{\mathbf{u}}{1+\Omega}, p\}(\tilde{\omega}, 0, m, l) \tag{1}$$

where $\mathbf{u}$ and p stand for the velocity and the pressure respectively. Here, ω is the mode frequency in the frame rotating with the elliptical deformation, $\tilde{\omega} = (\omega + m\Omega)/(1+\Omega)$, and m and l are azimuthal and "meridional" wavenumbers respectively (see Lacaze et al., 2004, for details). Due to this property, the dispersion relation solutions in the sphere with global rotation are the same as the ones given by Lacaze et al. (2004) without global rotation

when ω is replaced by $\tilde{\omega}$. The linear analysis of the elliptical instability in the rotating frame can thus be expressed from the results obtained without global rotation. The condition for resonance between two waves is simply given by $(m_2, \omega_2) = (m_1 + 2, \omega_1)$, and the corresponding excited resonance is labeled by (m_1, m_2). Note that as frequencies of normal modes are confined to the interval $m-2 < \tilde{\omega} < m+2$, resonances are only possible for Ω outside the range $[-3/2; -1/2]$. There, the growth rate $\sigma_1 = \sigma/\varepsilon$ is solution of the equation (see again Lacaze et al., 2004, for details)

$$\begin{aligned}\left(\sigma_1 \tilde{\mathcal{J}}_{1|1} - \sqrt{E}\nu_s^1 (1+\Omega)^2/\varepsilon - \tilde{\mathcal{C}}_{1|1}\right)\left(\sigma_1 \tilde{\mathcal{J}}_{2|2} - \sqrt{E}\nu_s^2 (1+\Omega)^2/\varepsilon - \tilde{\mathcal{C}}_{2|2}\right) \\ = \left(\tilde{\mathcal{N}}_{1|2} - (1+\Omega)\tilde{I}_1\right)\left(\tilde{\mathcal{N}}_{2|1} - (1+\Omega)\tilde{I}_2\right),\end{aligned} \tag{2}$$

where $\tilde{\mathcal{J}}_{i|i}$ corresponds to the norm of mode i, $\tilde{\mathcal{N}}_{i|j}$ to the coupling coefficient between modes i and j, ν_s^i to the viscous damping induced by the no-slip boundary condition on each mode derived from the work of Kudlick (1966)[1], and $\tilde{\mathcal{C}}_{i|i}$ to the possible detuning of the instability when Ω is slightly off the perfect resonance condition. The exact expressions of all these coefficients are given in appendix A.

Numerical resolution of equation (2) determines the growth rate of any given resonance depending on the dimensionless parameters (ε, Ω, E). Our computations demonstrate that only principal resonances characterized by the same meridional wavenumber (i.e. $l_1 = l_2$) lead to a significant positive growth rate, as already noted for non-rotating cases by Kerswell (1993)

[1]Note that only boundary layer effects are considered here, and that damping due to inner shear layers are neglected. This assumption has been fully justified by numerical computation for the spin-over mode (Hollerbach and Kerswell, 1995), and is supposed to remain valid here.

and Lacaze et al. (2004). An example of the resolution of equation (2) as a function of Ω is shown in figure 2(a) for the parameter range relevant to our experimental configuration. Each mode can be excited inside a resonance band in Ω where the growth rate is positive. When several resonances are possible at a given value of Ω, one expect the most unstable mode (i.e. the one with the largest growth rate) to be the first one excited. We also show in figures 2(b) and 2(c) the effects of eccentricity and Ekman number: decreasing ε implies narrower resonance bands, whereas decreasing the Ekman number allows the excitation of more resonances. In the limit of small Ekman numbers relevant to planetary and stellar systems, we find that there always exists an excitable resonance, except in the stable range $\Omega \in [-3/2; -1/2]$, corresponding in astrophysical terms to $\Omega_{spin}/\Omega_{orbit} \in [-1; 1/3]$. Besides, as shown in figure 2(c), its growth rate is correctly approximated by

$$\sigma_1 = \frac{(3+2\Omega)^2}{16(1+\Omega)^2} - c\frac{\sqrt{E}}{\varepsilon}, \tag{3}$$

where the first term on the right-hand side comes from the inviscid local analysis (Le Dizès, 2000) and where c is a constant of order 1, which can be explicitly computed for each resonance using equation (2).

2.2. Experimental results

A series of experiments was performed with a fixed eccentricity $\varepsilon = 0.16$ and various Ekman numbers in the range $[10^{-5}; 10^{-4}]$, systematically changing Ω_{orbit} and Ω_F to excite various resonances. Starting from rest, we first set the table's rotation to its assigned value Ω_{orbit}. Once solid body rotation is reached, the second motor controlling the fluid rotation is turned on. We

then observe the potential development of an instability using a video camera embedded on the table. As illustrated in figure 2(a), good agreement with the global analysis is found regarding the selected resonance: outside the stable range $\Omega \in [-3/2; -1/2]$, stationary $(-1, 1)$ mode with a sinusoidal rotation axis and various wavelengths as well as other more exotic modes recognized by their complex radial structure and/or by their periodic behavior (see figures 3 and 4) can be selected by changing the dimensionless ratio Ω only, providing the Ekman number is small enough. For each selected value of Ω, the first observed mode of instability corresponds to the most unstable mode by the theory (i.e. the one with the largest growth rate). In the vicinity of the threshold, the excited resonance induces a flow whose saturation amplitude rapidly grows with ε and Ω_F, until reaching a value comparable to the imposed rotation velocity $\Omega_F R$ (see for instance figure 5). At slightly smaller Ekman numbers or slightly larger ε, we then observe disordered patterns superimposed on the selected main flow (figure 5c,d). These patterns may induce the collapse of the selected mode on a very rapid timescale comparable to the rotation rate, and an intermittent behavior takes place. When several theoretical resonances are close to each other, we observed complex patterns originating from the superimposition or the succession in time of the different modes.

Note again that in the absence of global rotation, the only perfect resonance and the first destabilized mode in the vicinity of threshold is the spin-over mode. This is the first time that oscillatory modes such as the $(0, 2)$ one shown in figures 3 and $4a$ and the $(1, 3)$ one shown in figure $4b$ are experimentally observed in a sphere.

2.3. Estimates of power dissipation

Energy dissipated by tides in a planet is traditionally related to the dissipation of the induced shear flow by viscosity in its fluid part(s) and by anelasticity in its solid part(s): it is thus typically proportional to the square of the (small) tidal deformation ε. With the exception of Earth, where the prevalent source of dissipation is due to viscous friction of water tides on ocean floor (estimated power $2 \times 10^{12} W$), the fluid component of tidal dissipation usually remains negligible. However, we observe in our experiments that even if the tidal deformation is very small, its subsequent instability induces a flow over the whole system with a typical velocity comparable to the imposed rotation velocity $\Omega_F R$, as soon as $\varepsilon/\sqrt{E}$ is about 10 (see for instance figure 5 and the analytical model by Lacaze et al. (2004)). This is especially important when trying to estimate the energy dissipated by the elliptical instability.

Schematically, the intermittent behavior observed at small Ekman numbers in our experiment can be characterized by three stages. First, starting from the base flow (which can be either a laminar solid body rotation or a more turbulent state induced for instance by convection or differential rotation), the instability grows continuously on a typical time given by the growth rate, until it saturates to a typical velocity. Then, the selected mode breaks down into small scales in a very short timescale, comparable to some fluid's rotations and significantly smaller than the typical growth time of the instability (see also Lacaze et al., 2004). A new cycle then begins. Note that the energy dissipation related to this collapse has already been evaluated by several authors (Malkus, 1968; Vanyo, 1991; Kerswell, 1996; Kerswell and

Malkus, 1998) and leads to the estimate $P_{dissip} \sim \rho R^5 \Omega_F^3$ (this would correspond to an unrealistically huge amount of dissipation during the collapse breakdown, e.g. $P_{dissip} \sim 2 \times 10^{24} W$ in the Earth, but see the relevant discussion in Kerswell and Malkus (1998)). In the context of this paper, we focus on the continuous viscous dissipation during growth and saturation of the instability.

The energy necessary to excite and maintain the selected mode is supplied by the tidal deformation and by the relative angular velocity of the spherical container (i.e. the rigid mantle in the case of a planet) compared to tides. Following the model of Vanyo and Likins (1972) developed in the closely related case of precession, one may consider that this energy is transmitted to the fluid (i.e. the liquid core in the case of a planet) through a thin viscous boundary layer at the solid-liquid interface. In the absence of orbital velocity, the spin-over mode takes place, similarly to the case of precession, and we may consider the "rigid sphere approximation" introduced in Vanyo and Likins (1972): the interior portion of the fluid is assumed to behave as a perfectly rigid sphere rotating at $\mathbf{\Omega_{spin}} + \mathbf{\Omega_{SO}}$, where $\mathbf{\Omega_{SO}}$ is the spin-over mode. The moment of the container acting on the fluid can then be expressed as

$$\mathbf{C^{m/c}} = -2M\nu \frac{R}{h} \mathbf{\Omega_{SO}}, \tag{4}$$

where M is the mass of the fluid and h the size of the viscous boundary layer, taken as $h = \sqrt{\nu/\Omega_{SO}}$. The power dissipated by the whole system (i.e. the container rotating at $\mathbf{\Omega_{spin}}$ plus the fluid rotating at $\mathbf{\Omega_{spin}} + \mathbf{\Omega_{SO}}$) is then simply given by

$$P_{ell} = \mathbf{\Omega_{SO}} \cdot \mathbf{C^{m/c}} = -2M\nu \frac{R}{h} \Omega_{SO}^2, \tag{5}$$

Replacing Ω_{SO} by $\Omega_{spin}\omega_{SO}$, where ω_{SO} is the dimensionless spin-over mode amplitude which typically ranges between 0 (below threshold of the tidal instability) and 1 (far from threshold of the tidal instability), the dissipated power is written

$$P_{ell} = -2MR\sqrt{\nu}|\Omega_{spin}|^{5/2}|\omega_{SO}|^{5/2}. \quad (6)$$

The non-linear evolution of ω_{SO} as a function of time and its dependence on ε and E have been modeled theoretically by Lacaze et al. (2004) for the laminar mode, in close agreement with experimental results. We are thus in position to evaluate the energy dissipation P_{ell} for the spin-over mode. In the more general case where orbital velocity is present, the energy necessary for the instability comes from the difference between the spin velocity and the rotation velocity of the tides (i.e. the orbital velocity) and one may reasonably expect the dissipated power to be

$$P_{ell} = -2M\sqrt{\nu}|\Omega_{spin} - \Omega_{orbit}|^{5/2}|\omega_{ell}|^{5/2}. \quad (7)$$

Here, ω_{ell} is the dimensionless amplitude of the selected resonance, which should be comparable to the amplitude of the spin-over mode for the same values of eccentricity and Ekman number. Note that at large value of ε or small value of E, this calculation will represent a lower bound, since it does not take into account the additional turbulent dissipation coming from the chaotic motions superimposed on the large scale mode (see figure 5).

Evaluation of P_{ell} for the Earth is difficult because its core is just at the vicinity of the threshold for instability, where ω_{ell} rapidly changes from 0 to 1 (Lacaze et al., 2006). Following Aldridge et al. (1997), if we suppose that the growth rate of the instability is correctly approximated by the classical

formula $\sigma = 0.5\varepsilon - 2.62\sqrt{E}$ and that the typical growth rate of the instability in the Earth ranges between 10^3 and 10^6 years, the dissipation due to the (laminar) tidal instability ranges between $P_{ell} \sim 10^9 W$ and $P_{ell} \sim 2 \times 10^5 W$ respectively. It thus remains relatively small compared to the viscous dissipation by water tides on ocean floor (typically $2 \times 10^{12} W$), which is supposed to be the dominant effect in the case of the Earth. Let us now look at Jupiter's moon Io. As explained for instance in Kerswell and Malkus (1998), Io is almost synchronized in its revolution around Jupiter, but orbital resonances with Europa and Ganymede force it to follow a slightly elliptical orbit of eccentricity $\beta = 0.004$. As a result, the tidal bulge raised by Jupiter, of magnitude $\epsilon \sim 6 \times 10^{-3}$, oscillates back and forth across Io's body with a typical angular velocity $\Omega_{orbit} = \Omega_{spin}(1 - 2\beta \cos(\Omega_{spin} t))$. With the characteristic values for Io tides given by Kerswell and Malkus (1998), one then finds that the elliptical instability almost saturates at its maximum value (i.e. $\omega_{ell} = 0.99$) and $P_{ell} \sim 4 \times 10^9 W$ at saturation, i.e. a large dissipation for fluid motion, but negligible compared to the estimated tidal dissipation in Io's mantle (i.e. $O(10^{14}) W$). However this value corresponds to the present state of Io (i.e. almost synchronized) and does not preclude that tidal dissipation may have had a first order influence in the past, especially during its evolution towards synchronization.

3. A fully coupled model of synchronization of stellar and planetary binary systems

Our theoretical study, confirmed by laboratory experiments, highlights several points directly relevant to synchronizing stellar and planetary binary

systems. Provided that $\sqrt{E}/\varepsilon << 1$ (which is usually the case for moons and close binary stars, and which may be the case for some planetary cores), we conclude from the previous section that (i) a mode of the elliptical instability will always be excited, except when $\Omega_{spin}/\Omega_{orbit} \in [-1; 1/3]$, that (ii) its growth rate is correctly approximated by equation (3) with a constant $1 < c < 10$, that (iii) the induced fluid motion may take various and complex forms, and that (iv) the tidal instability may generate first order motions. As opposed to our experiments where spinning and orbital angular velocities are imposed by two motors, the energy dissipation related to these motions in natural configuration implies an evolution of the binary system towards synchronization. To further illustrate and quantify this effect, we now examine a fully coupled model of tidal synchronization based on our theoretical and experimental results. Note again that in the limit $\sqrt{E}/\varepsilon << 1$, resonance bands are dense in the $\Omega_{spin}/\Omega_{orbit}$ space, except in the stable range $\Omega_{spin}/\Omega_{orbit} \in [-1; 1/3]$. We thus suppose that during the evolution, the instability jumps from one resonance band to the following one while always remaining at saturation. In particular, we do not consider any cyclic behavior with growing and breakdown phases of the instability, as observed in our experiments with unaltered forcing.

We consider two spinning bodies of radius R_i and mass M_i orbiting on a circular trajectory of radius a. We note I_i and $\Omega_{spin,i}$ the moment of inertia and the angular velocity of the mantle of body i, and $I_{core,i}$ and $\Omega_{core,i}$ the moment of inertia and the angular velocity of the core of body i. The tidal deformation of body 1 by body 2 is given in the limit of hydrostatic equilibrium by $\epsilon = \frac{3}{2}\frac{M_2}{M_1}(\frac{R_1}{a})^3$. The evolution of this system is described by

two coupled equations, corresponding to the conservation of total angular momentum

$$L = \frac{M_1 M_2}{M_1 + M_2} a^2 \Omega_{orbit} + I_1 \Omega_{spin,1} + I_{core,1} \Omega_{core,1} + I_2 \Omega_{spin,2} + I_{core,2} \Omega_{core,2}, \quad (8)$$

and to the decrease of mechanical energy

$$E = -\frac{G M_1 M_2}{2a} + \frac{1}{2} I_1 \Omega_{spin,1}^2 + \frac{1}{2} I_{core,1} \Omega_{core,1}^2 + \frac{1}{2} I_2 \Omega_{spin,2}^2 + \frac{1}{2} I_{core,2} \Omega_{core,2}^2 \quad (9)$$

because of tidal dissipation (see for instance Rieutord, 2003). As opposed to our experiments, the synchronizing system evolves from one resonance to another as the spin and orbital velocities continuously change. We suppose that the mode remains at saturation during this evolution, and thus approximate the tidal dissipation in the core of each body by (7) at saturation. The amplitude of the mode is given by the corresponding value of the spin-over mode determined by Lacaze et al. (2004).

Let's now assume that body 1 corresponds to a typical moon with a 50% core orbiting a large planet (for instance Io in the vicinity of Jupiter). Then, the much heavier body 2 evolves on a much longer timescale, and the spin and core velocities of body 2 in equations (8) and (9) can be taken as constant. Besides, the angular momentum of the moon core typically corresponds to 10% of the angular momentum of its mantle, and core terms can be neglected in equations (8) and (9) to keep the problem simple. Then, using equation (8) and the third Kepler law (i.e. $\Omega_{orbit}^2 a^3 = G(M_1 + M_2)$, where G is the gravitational constant) to eliminate the orbital velocity and radius, the energy equation $dE/dt = -P_{ell}$ can easily be reduced to a single equation for the spin angular velocity

$$\frac{d\Omega_{spin,1}}{dt} = -\frac{2 M_c \nu^{1/2}}{I_1} |\omega_{ell}|^{5/2} |\Omega_{spin,1} - \Omega_{orbit}|^{1/2} (\Omega_{spin,1} - \Omega_{orbit}), \quad (10)$$

$$\text{and} \quad a = \left(a_0^{1/2} + \frac{I_1(\Omega_{spin,1}^{init} - \Omega_{spin,1})}{M_1 (G M_2)^{1/2}} \right)^2, \quad \Omega_{orbit} = \left(\frac{G M_2}{a^3} \right)^{1/2}, \qquad (11)$$

where M_c is the mass of the liquid core of body 1, $\Omega_{spin,1}^{init}$ its initial spinning angular velocity and a_0 the initial orbital radius. The $(\Omega_{spin,1} - \Omega_{orbit})$ factor on the right-hand side of equation (10) implies that the system systematically evolves towards the equilibrium state of synchronization (i.e. $\Omega_{spin,1} = \Omega_{orbit}$).

The evolution of a typical body equivalent to Jupiter's moon Io is shown in figure 6 for three different initial conditions. When the tidal instability is present, the evolution takes place on very short time scales of 10000 years, and comes from energy dissipation as large as 100 times the present dissipation by Io's mantle. Besides, figure 6 illustrates the following general rules. A slow or moderately fast prograde moon (i.e. $\Omega_{spin,1}^{init}/\Omega_{orbit}^{init} > 1/3$, solid line) always excites elliptical instability and thus evolves rapidly towards synchronization. A slow retrograde moon (i.e. $\Omega_{spin,1}^{init}/\Omega_{orbit}^{init} < -1$, dashed line) initially excites a resonance and thus evolves rapidly towards antisynchronization (i.e. $\Omega_{spin,1} = -\Omega_{orbit}$), where no resonance is possible anymore. Finally, a fast retrograde or very fast prograde moon (i.e. $-1 < \Omega_{spin,1}^{init}/\Omega_{orbit}^{init} < 1/3$, dotted line) cannot excite any resonance. Note that in the last two cases, the system should evolve because of other processes not considered here (e.g. solid dissipation, viscous diffusion of the tidal shear, ...) and will ultimately reach the domain of elliptical instability. However, it would be very interesting to perform a systematic analysis of the ratio $\Omega_{spin}/\Omega_{orbit}$ for all moons and planets in planetary systems, in order to verify the potential impact of the zone of slow evolution $\Omega_{spin}/\Omega_{orbit} \in [-1; 1/3]$.

4. Conclusion

In this paper, combining theoretical and experimental approaches, we have systematically characterized the various and complex resonances excited by tidal instability in planetary liquid cores and stars, depending on their relative orbital and spinning angular velocities. We have also demonstrated that tidal instability may play a dominant role in the synchronization process of stellar and planetary binary systems. Of course, our approach is highly simplified, regarding both the structural model of the binary system as well as the estimated power dissipated by tides. Moreover, the elliptical instability studied here will compete in natural configurations with various other phenomena, such as stable stratification and convection (see for instance the study of the interaction between the elliptical instability and thermal effects in Le Bars and Le Dizès, 2006), or solidification (a solid inner core amplifies the viscous dissipation by the generation of detached shear layers, e.g. Rieutord et al., 2001, but should appear on a longer time scale according to the orders of magnitude found here). One should also notice that our present study focus on hydrodynamical aspects of the tidal instability only, neglecting Lorentz forces related to planetary or stellar magnetic fields. This simplification is fully justified in the case of Io (see Herreman et al., 2009), but magnetic effects may be predominant in other situations. Anyway, the key point demonstrated here is that even if the tidal deformation is very small, its subsequent instability may have a velocity amplitude of first order over the whole domain and takes various and complex forms. As a result, it appears that its influence should not be neglected or oversimplified when describing the dynamics of planetary cores and stars, or when tackling other

problems relevant at the planetary and stellar scales, such as core cooling and dynamo process.

Appendix A : notations.

The operators appearing in equation (2) are defined as follows.

Volume terms $\tilde{\mathcal{J}}_{i|i}$, $\tilde{\mathcal{N}}_{i|j}$ and $\tilde{\mathcal{C}}_{i|i}$ respectively correspond to the norm of mode i, to the coupling coefficient between modes i and j, and to the detuning of the instability when Ω is slightly off the perfect resonance condition. They are computed using the scalar product

$$\tilde{\mathcal{X}}_{i|j} = \int\int \bar{\mathbf{u}}_i^0 \cdot \tilde{\mathcal{X}} \mathbf{u}_j^0 r dr dz$$

applied respectively to the operators

$$\mathcal{J} = \begin{pmatrix} 1 & 0 & 0 & 0 \\ 0 & 1 & 0 & 0 \\ 0 & 0 & 1 & 0 \\ 0 & 0 & 0 & 0 \end{pmatrix} \quad \mathcal{N} = \begin{pmatrix} D-1 & 0 & 0 & 0 \\ -2I & D+1 & 0 & 0 \\ 0 & 0 & D & 0 \\ 0 & 0 & 0 & 0 \end{pmatrix} \quad \mathcal{C} = \begin{pmatrix} 0 & 2\Omega & 0 & 0 \\ -2\Omega & 0 & 0 & 0 \\ 0 & 0 & 0 & 0 \\ 0 & 0 & 0 & 0 \end{pmatrix}.$$

Here, $D = -\dfrac{\partial}{\partial r} - I\dfrac{\partial}{\partial \theta}$, $I^2 = -1$, and the vectors $\mathbf{u}^0$ are defined as

$$\mathbf{u}^0 = \begin{pmatrix} u^0 \\ v^0 \\ w^0 \\ p^0 \end{pmatrix}$$

and correspond to the configuration without global rotation (see Lacaze et al., 2004).

Surface terms ν_s^j and $\tilde{I}_j$ respectively correspond to the viscous dissipation close to the solid boundary estimated using the work of Kudlick (1966) and to surface effect induced by the elliptic shape of the boundary. They are given by

$$\tilde{I}_1 = \int_{-1}^{1} p_1^0 \left(-I\frac{(1-z^2)}{4}\frac{\partial u_2^0}{\partial r} + \frac{(1-z^2)^{1/2}}{2} v_2^0 - I\frac{z(1-z^2)}{4}\frac{\partial w_2^0}{\partial r} - I\frac{z}{4} w_2^0 \right) dz,$$

$$\tilde{I}_2 = \int_{-1}^{1} p_2^0 \left(I\frac{(1-z^2)}{4}\frac{\partial u_1^0}{\partial r} + \frac{(1-z^2)^{1/2}}{2} v_1^0 + I\frac{z(1-z^2)}{4}\frac{\partial w_1^0}{\partial r} + I\frac{z}{4} w_1^0 \right) dz,$$

$$\text{and } \nu_s^j = \int_{Sphere} \nabla^* p_j^0 \cdot \mathcal{L} dS,$$

where $\nabla^* = (\partial/\partial r, -Im/r, \partial/\partial z)$,

$$\mathcal{L} = \begin{pmatrix} -\frac{1}{2}\left(\frac{Q_+}{-p_+} + \frac{Q_-}{-p_-}\right) \\ -\frac{I}{2\cos\phi}\left(\frac{Q_+}{-p_+} - \frac{Q_-}{-p_-}\right) \\ -\frac{\tan\phi}{2}\left(\frac{Q_+}{-p_+} + \frac{Q_-}{-p_-}\right) \end{pmatrix},$$

$$p_\pm = \frac{1 + I\ \text{sign}\left((1+\Omega)(-\frac{\omega-m}{1+\Omega} \pm 2\cos\phi)\right)}{\sqrt{2}} \sqrt{|(1+\Omega)(-\frac{\omega-m}{1+\Omega} \pm 2\cos\phi)|},$$

$$\text{and } Q_\pm = u^0 \pm I v^0 \cos\phi.$$

References

Aldridge, K., Seyed-Mahmoud, B., Henderson, G., van Wijngaarden, W., 1997. Elliptical instability of the Earth's fluid core. Phys. Earth Planet. Int. 103, 365–74.

Herreman, W., Le Bars, M., Le Gal, P., 2009. On the effects of an imposed magnetic field on the elliptical instability in rotating spheroids. Phys. Fluids 21, 046602.

Hollerbach, R., Kerswell, R. R., 1995. Oscillatory internal shear layers in rotating and precessing flows. J. Fluid Mech. 298, 327–339.

Kerswell, R. R., 1993. The instability of precessing flow. Geophys. Astrophys. Fluid Dyn. 72, 107–144.

Kerswell, R. R., 1996. Upper bounds on the energy dissipation in turbulent precession. J. Fluid Mech. 321, 335–370.

Kerswell, R. R., 2002. Elliptical instability. Annual Review of Fluid Mechanics 34, 83–113.

Kerswell, R. R., Malkus, W. V. R., 1998. Tidal instability as the source for Io's magnetic signature. Geophys. Res. Lett. 25, 603–6.

Kudlick, M., 1966. On the transient motions in a contained rotating fluid. PhD thesis, MIT.

Lacaze, L., Herreman, W., Le Bars, M., Le Dizès, S., Le Gal, P., 2006. Magnetic field induced by elliptical instability in a rotating spheroid. Geophys. Astrophys. Fluid Dyn. 100, 299–317.

Lacaze, L., Le Gal, P., Le Dizès, S., 2004. Elliptical instability in a rotating spheroid. J. Fluid Mech. 505, 1–22.

Le Bars, M., Le Dizès, S., 2006. Thermo-elliptical instability in a rotating cylindrical shell. J. Fluid Mech. 563, 189–198.

Le Bars, M., Le Dizès, S., Le Gal, P., 2007. Coriolis effects on the elliptical instability in cylindrical and spherical rotating containers. J. Fluid Mech. 585, 323–342.

Le Dizès, S., 2000. Three-dimensional instability of a multipolar vortex in a rotating flow. Phys. Fluids 12, 2762–74.

Malkus, W. V. R., 1968. Precession of the Earth as the cause of geomagnetism. Science 160, 259–264.

Rieutord, M., 2003. Evolution of rotation in binaries: physical processes. Stellar Rotation, Proc. IAU Symp. 215, 394–403.

Rieutord, M., Georgeot, B., Valdettaro, L., 2001. Inertial waves in a rotating spherical shell: attractors and asymptotic spectrum. J. Fluid Mech. 435, 103–144.

Vanyo, J. P., 1991. A geodynamo powered by luni-solar precession. Geophys. Astrophys. Fluid Dyn. 59, 209–234.

Vanyo, J. P., Likins, P. W., 1972. Rigid-body approximations to turbulent motion in a liquid-filled, precessing spherical cavity. J. Appl. Mech., 39, 18–24.

Waleffe, F. A., 1990. On the three-dimensional instability of strained vortices. Phys. Fluids 2, 76–80.

Figure 1: *(a) Sketch of the experimental set-up and (b) correspondence with the geophysical configuration (top view).*

Figure 2: *(a) Viscous growth rate as a function of* Ω*, determined analytically for the first 21 principal resonances of the* $(-1,1)$ *mode (continuous lines), of the* $(0,2)$ *mode (dashed lines) and of the* $(1,3)$ *mode (dotted lines), for fixed values of eccentricity* $\varepsilon = 0.16$ *and Ekman number* $E = 1.7 \times 10^{-4}$*. Symbols stand for the location of experimentally observed resonances, with triangles corresponding to* $(-1,1)$ *modes, stars to* $(0,2)$ *modes and squares to* $(1,3)$ *modes. (b) The same for* $\varepsilon = 0.16$*,* $E = 1.7 \times 10^{-8}$ *and (c)* $\varepsilon = 0.016$*,* $E = 1.7 \times 10^{-8}$*. Also shown in (c) is the approximated growth rate given by equation (3), using two extreme values* $c = 0$ *and* $c = 10$*. Note that in the limit* $\sqrt{E}/\varepsilon << 1$*, resonance bands are dense in the* Ω *space, except in the stable range* $\Omega \in [-3/2; -1/2]$*. The false impression that holes without resonance could be created in (c) only comes from the fact that we restrain our computations to the first* 63 *resonances.*

Figure 3: *Time sequence of the periodic* $(0,2)$ *mode excited in our experiment for* $\varepsilon = 0.16$*,* $E = 4.5 \times 10^{-4}$ *and* $\Omega = -0.20$ *(i.e.* $\Omega_F = 4.7 rad/s$ *and* $\Omega_{orbit} = -0.94 rad/s$*).*

Figure 4: *Spatiotemporal diagrams obtained by extracting the same line parallel to the rotation axis in each image of a given video sequence: (a)* $(0,2)$ *mode excited in our experiment for* $\varepsilon = 0.16$*,* $E = 4.5 \times 10^{-4}$ *and* $\Omega = -0.20$ *(i.e.* $\Omega_F = 4.7 rad/s$ *and* $\Omega_{orbit} = -0.94 rad/s$*) and (b) (1,3) mode excited in our experiment for* $\varepsilon = 0.16$*,* $E = 3.4 \times 10^{-4}$ *and* $\Omega = -0.11$ *(i.e.* $\Omega_F = 6.2 rad/s$ *and* $\Omega_{orbit} = -0.68 rad/s$*). The measured mode pulsations are respectively* $\omega = 4.4 rad/s$ *and* $\omega = 12.6 rad/s$*, in good agreement with the theoretical predictions.*

Figure 5: *Kalliroscope visualization of the elliptical instability for a fixed Ekman number* $E = 10^{-5}$ *and increasing values of* ε *(note that these four pictures were obtained in a* $20cm$ *in diameter sphere). The effective rotation axis of the fluid is clearly visible, coming from the superimposition of the imposed vertical rotation and the spin-over mode. Hence, the inclination angle is an indication of the ratio between the mode amplitude and the imposed rotation. It seems to saturate for* $\varepsilon/\sqrt{E} > 0(10)$*, where the instability induces velocity perturbations comparable to the imposed rotation velocity. Further increasing* ε*, the flow becomes more and more complex at small scale where disordered motions take place. However, the spin-over mode remains present at large scale. The same behavior is observed when decreasing the Ekman number. Such an organization of the flow with a large scale excited mode with first order velocities and superimposed three dimensional turbulence is expected at the planetary scale, for instance in Io's core.*

Figure 6: *Evolution of a typical moon corresponding to Io under the influence of Jupiter's tides (i.e.* $M_1 = 8.93 \times 10^{22} kg$*,* $M_2 = 1.90 \times 10^{27} kg$*,* $a_0 = 421800 km$*,* $R_1 = 1840 km$ *with a* 50% *core,* $I_1 = 1.2 \times 10^{35} kg.m^2$*,* $\nu = 10^{-6} m^2 s^{-1}$*) for three different initial spinning angular velocities, corresponding to a slow prograde moon (*$\Omega^{init}_{spin,1}/\Omega^{init}_{orbit} = 4$*, solid line), to a slow retrograde moon (*$\Omega^{init}_{spin,1}/\Omega^{init}_{orbit} = -4$*, dashed line) and to a rapid moon (*$\Omega^{init}_{spin,1}/\Omega^{init}_{orbit} = 1/4$*, dotted line): (a) evolution of the distance between Io and Jupiter in comparison with the initial distance* $a_0 = 421800 km$*, (b) evolution of the ratio between the spin and orbital angular velocities and (c) dissipated power by the elliptical instability.*

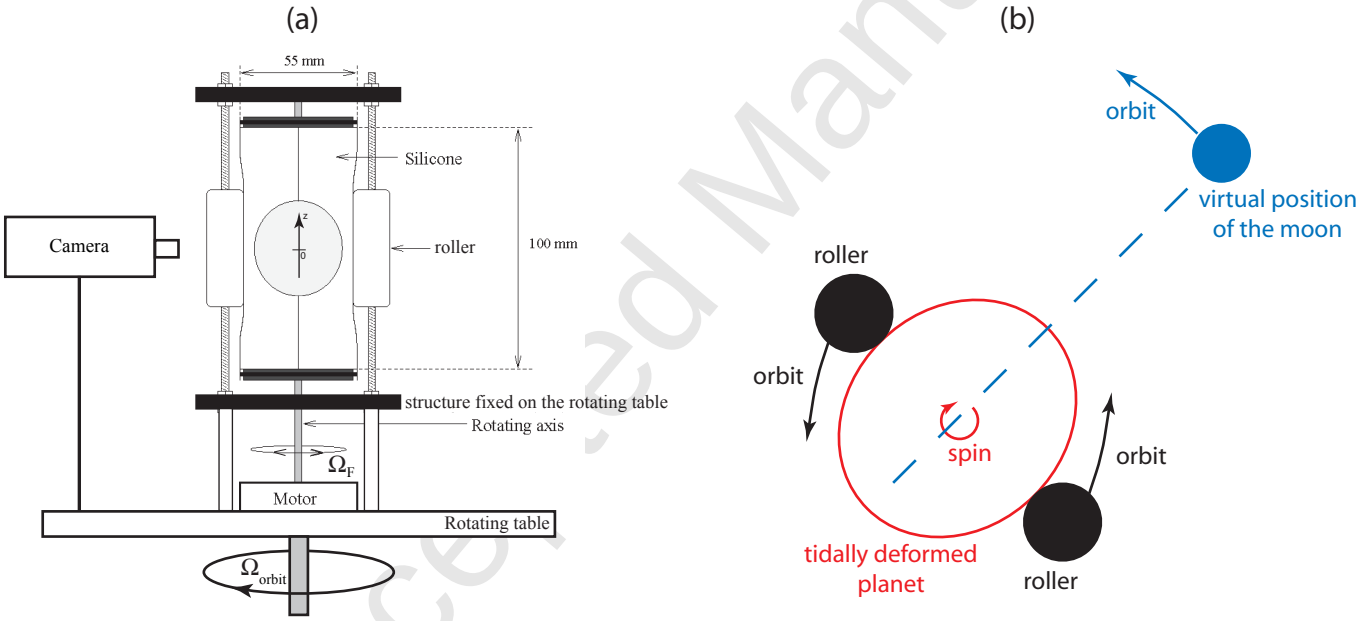

Figure 1

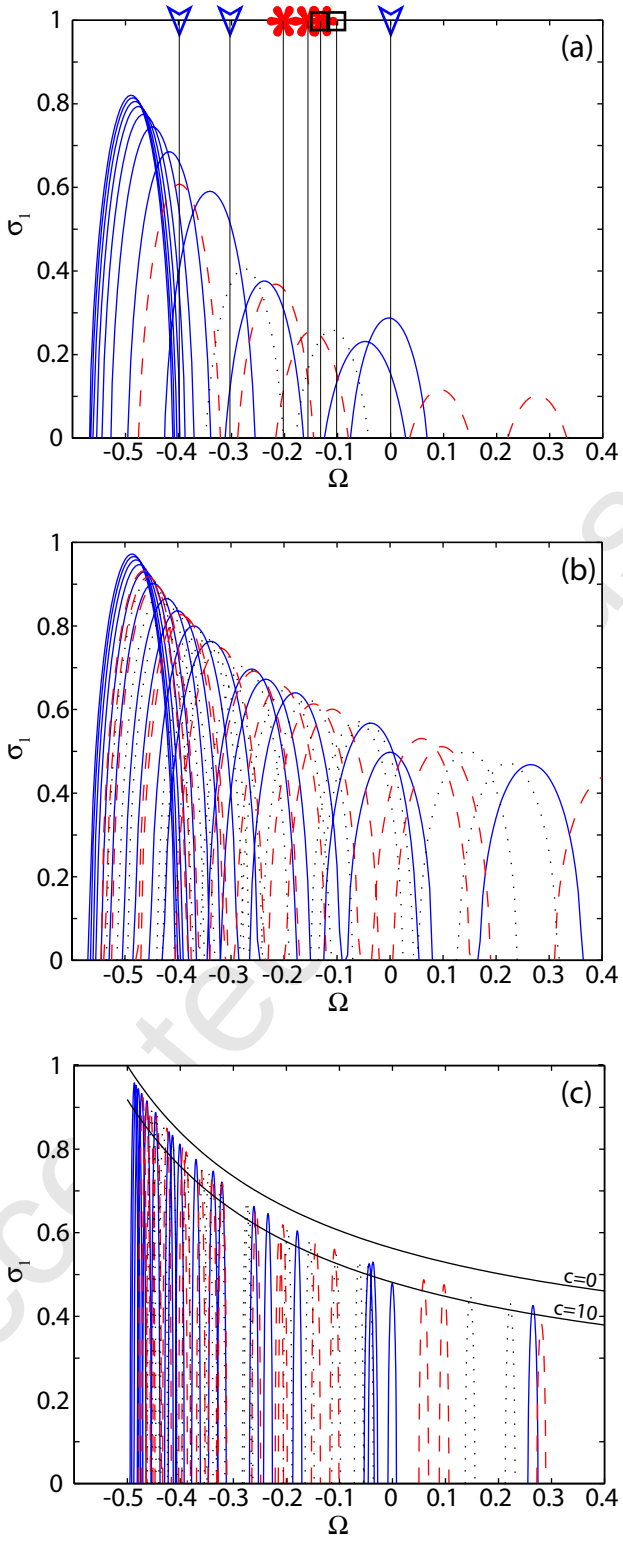

Figure 2

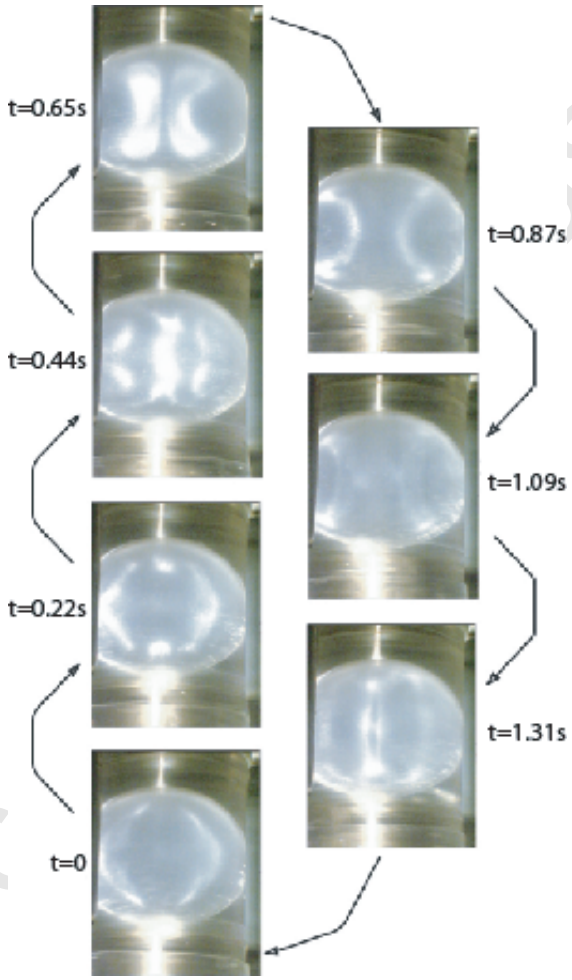

Figure 3

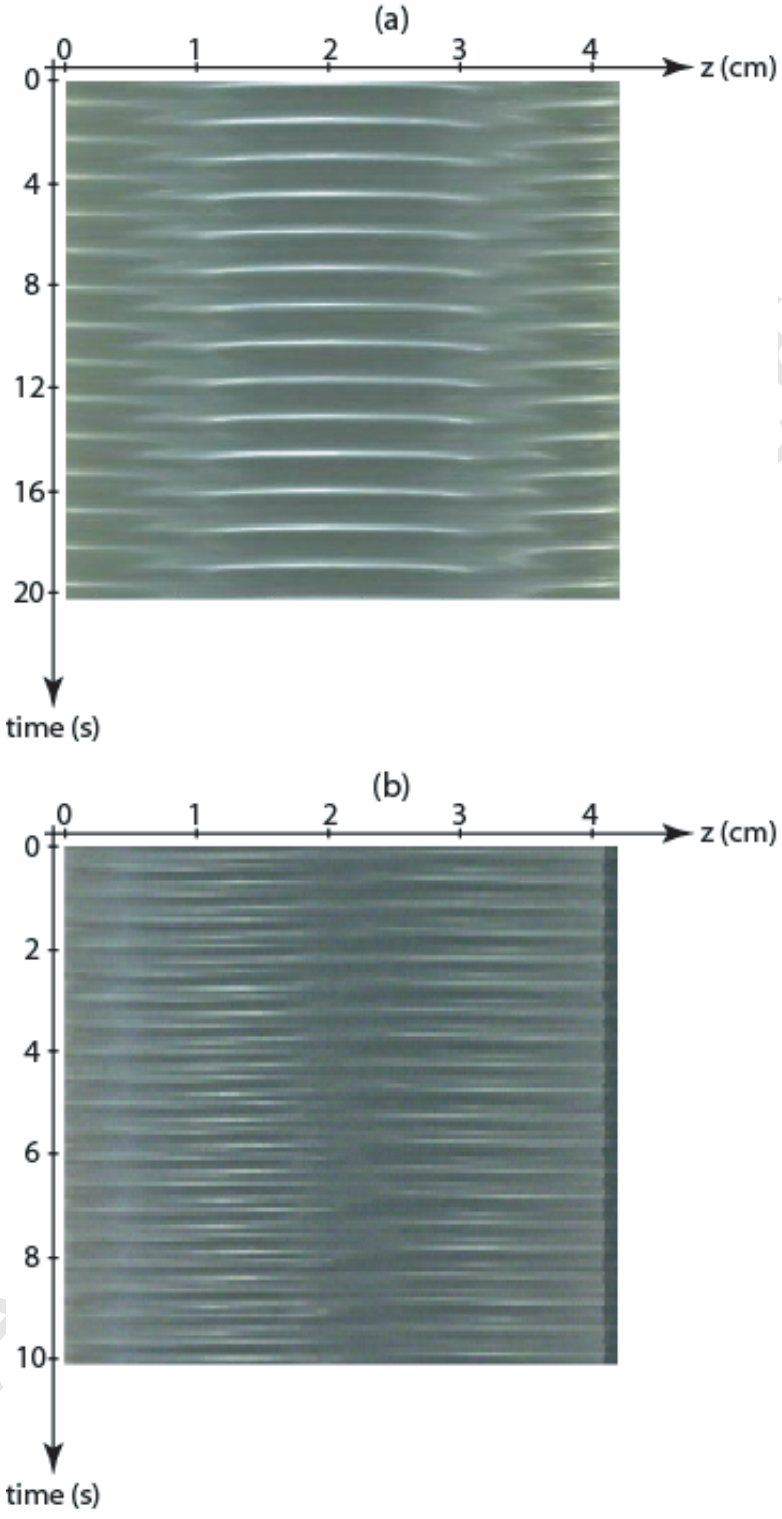

Figure 4

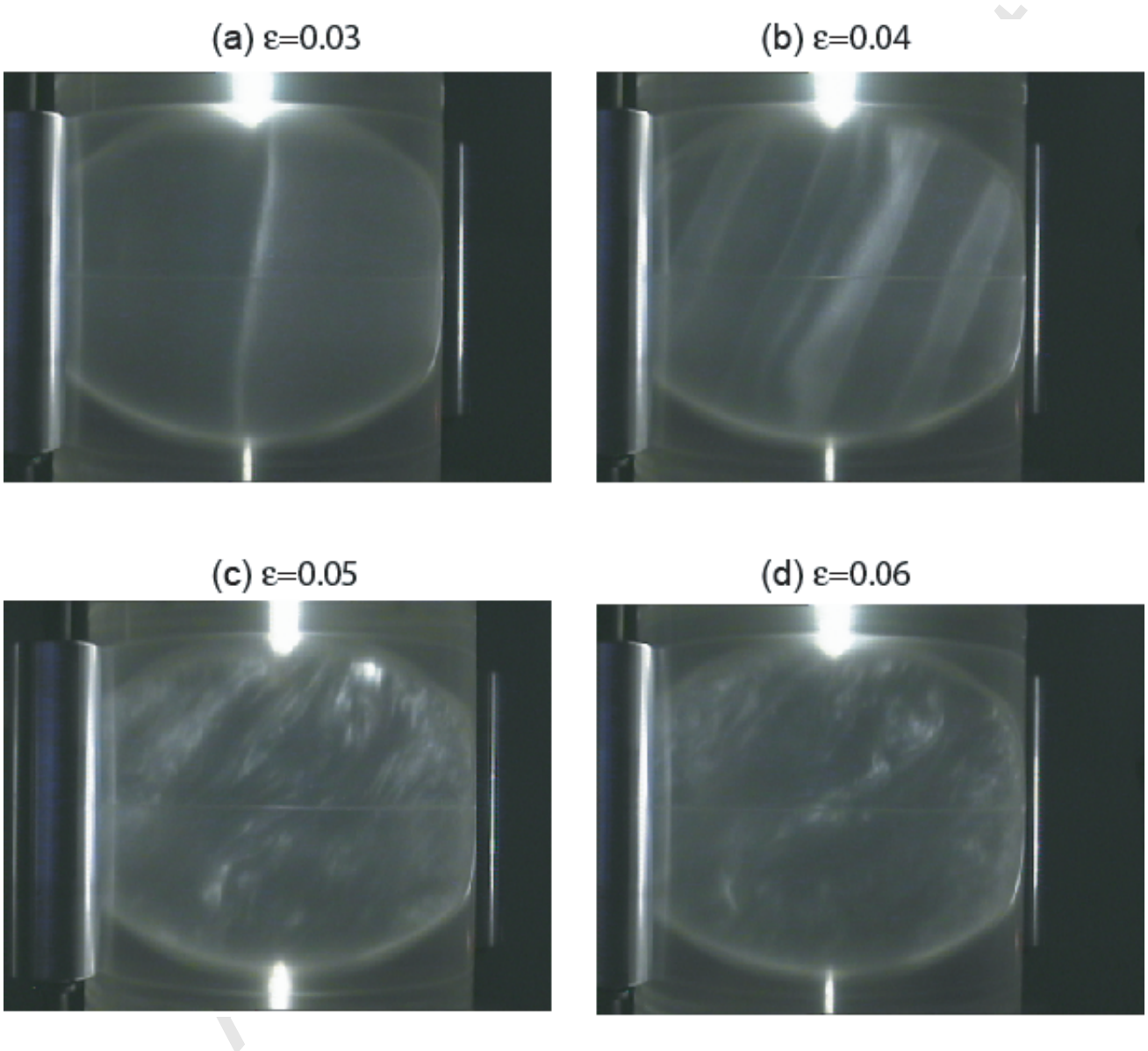

Figure 5

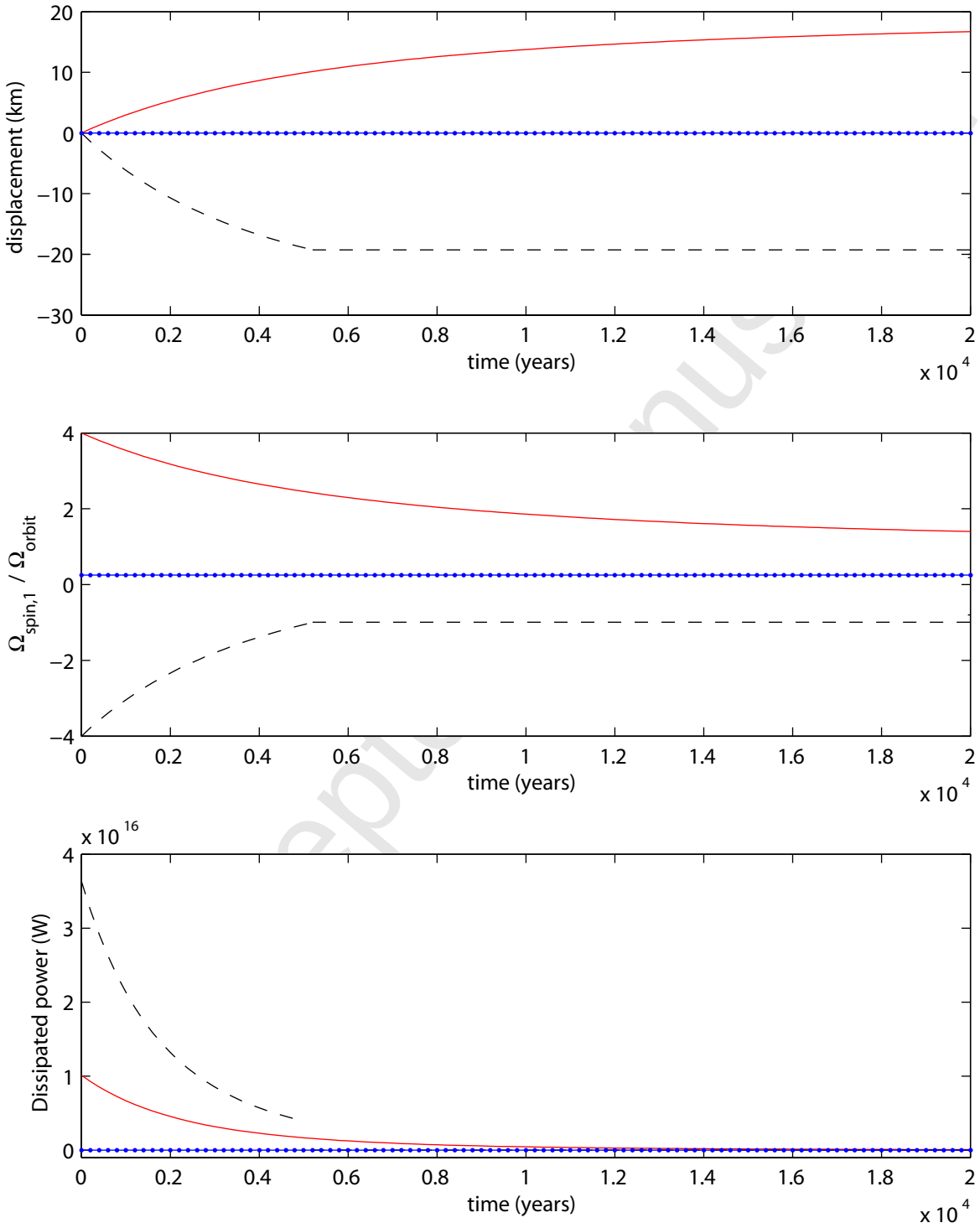

Figure 6